Master equation for the probability distribution functions of overlaps between particles in two dimensional granular packings

Kuniyasu Saitoh, Vanessa Magnanimo, and Stefan Luding
Faculty of Engineering Technology, MESA+, University of Twente, 7500 AE Enschede, The Netherlands
(Dated: November 8, 2013)

How does the force-chain-network in a random granular material react to hydrostatic compression? We show that not only contacts, but also their opening and closing as well as interparticle gaps, *i.e. virtual contacts*, must be included for a comprehensive description of the system response involving the probability distribution functions (PDFs) of the extended force network. Considering overlaps/forces as stochastic variables, their conditional probability distributions (CPDs) are (numerically) determined and allow to formulate a Master equation for the PDFs. The insight one gets from the CPDs is striking: The mean change of contacts reflects non-affinity, while their fluctuations obey uncorrelated Gaussian statistics. In contrast, virtual contacts are mostly affine to isotropic (de)compression in average, but show multi-scale correlations with considerable probability of large "jumps" according to a stable distribution (*cf.* Lévy distribution), that allows for a generalized central limit theorem. Noting that all changes of the network during compression are similarly scaled by the distance from the jamming density, the evolution of the system is fully described by the Master equation.

PACS numbers: 45.70.Cc,46.65.+g,61.43.-j

The statistical physics of soft matter, due to disorder, glassy dynamics, dissipation, etc. poses many difficulties for research and has wide practical applications. As one example, jammed granular assemblies are inherently out of equilibrium due to the dissipation of energy and the absence of temperature [1]. Despite their non-equilibrium nature, static properties of them around the rigidity transition density ϕ_J have been widely investigated as well as their relation to critical phenomena [2–5]. It is challenging to explain these observations on static granular packings by statistical mechanics, *e.g.* based on the Edwards ensemble [6] or force ensemble [7, 8], where all configurations of particles are equally probable under a constant volume or force and torque balances of particles, respectively. Further studies [9, 10] and comparison [11] of these ideas lead us to the exploration into the statistical weight, *i.e.* the probability distribution functions (PDFs), of forces. Many theoretical investigations [12–14] have been devoted to determine the functional forms of the PDFs obtained through experiments [15–17] and numerical simulations [18–20]. There is, however, still much debate about the tails of the PDFs [21] and how the closing/opening of contacts affects the PDFs at small forces [22–24]. In addition, we lack a more general description of the PDFs from the point of view of probability theory involving stochastic processes, the central limit theorem, and so on.

In this Letter, we take a different approach from the previous works based on the mechanical equilibrium of static packings. We regard overlaps between particles as *stochastic variables* and measure their conditional probability distributions (CPDs) by molecular dynamics (MD) simulations under isotropic (de)compression. The CPDs show striking features of not only contacts, but also closing/opening of contacts as well as interparticle gaps, *i.e. virtual contacts*. We introduce the Master equation for the PDFs of overlaps, where good agreement between its solutions and the PDFs obtained through MD simulations is established, as long as the increment of the area fraction $\delta\phi$ is much smaller than the distance from the jamming point $\phi - \phi_J$. Interestingly, the solutions are independent of history (the Markov property) and reversible if an effective increment $\gamma = \delta\phi/(\phi - \phi_J)$, which governs the amplitude of non-affine response, is small enough. Our stochastic approach opens the door to a new physical description of static granular packings.

We use MD simulations of two-dimensional frictionless granular particles. The normal force between particles in contact is given by $f = kx - \eta\dot{x}$ $(x > 0)$ with a spring constant k, viscosity coefficient η, overlap x and relative speed $\dot{x}$ in normal direction. A global damping force $\mathbf{f}_\mathrm{d} = -\eta\mathbf{v}$, proportional to the particle's velocity $\mathbf{v}$, is also introduced to enhance the relaxation. We prepare static packings of the particles by a method similar to the one used in Ref. [25]. At first, we randomly distribute a $50:50$ binary mixture of N particles with different radii, R and ρR $(\rho = 1.4)$, and the same masses m in a square periodic box, where each pair of particles is not in contact. Then, we adjust the size of the particles by rescaling each radius as $R(t+\delta t) = [1 + \{\bar{x} - x_\mathrm{m}(t)\}/l]R(t)$ until a target mean overlap $\bar{x}$ is obtained, where t, δt, and $x_\mathrm{m}(t)$ are time, an increment of time, and the mean overlap over all particles at time t, respectively, and the initial radius $R(0)$ corresponds to R or ρR. Here, we keep the mass constant and use a long length scale $l = 10^2 R$ to grow the particles gently [26]. The particles lose their kinetic energies by means of inelastic contacts and global damping. We stop rescaling each radius when the accelerations of all particles drops below a small threshold $10^{-6}kR/m$ and assume that the system is static [25]. We prepare 10

samples for smaller systems ($N = 512, 2048, 8192$) and 2 samples for the largest system ($N = 32768$) by changing the initial random configuration of particles. However, we only report the results of $N = 8192$ and note that all results do not depend on the system size. In our simulations, the jamming point ϕ_J obeys the scaling $\bar{x}(\phi) = A(\phi - \phi_J)^\alpha$ [4], where we find $\alpha = 1.0 \pm 0.002$, $\phi_J = 0.8458 \pm 0.0001$, and $A = (0.9 \pm 0.003)R_{\rm m}$ with the mean radius $R_{\rm m}$. Thus, the mean overlap is equivalent to the distance from the jamming point $\bar{x}(\phi) \simeq A(\phi - \phi_J)$.

We apply isotropic compression to each packing by rescaling every radius by $\sqrt{1 + \delta\phi/\phi}$ so that the area fraction changes from ϕ to $\phi + \delta\phi$. If an affine response of the packing is assumed [27], an overlap or interparticle gap $x(\phi)$, defined as the difference between the sum of the radii and the interparticle distance d, changes to $x_{\rm affine}(\phi+\delta\phi) = x(\phi)+(d/2\phi)\delta\phi$ [28]. However, the particles are randomly arranged and the force balance of each particle is broken by compression. Thus, the system relaxes to a new static state and the overlap or gap changes to a new value $x(\phi+\delta\phi) \neq x_{\rm affine}(\phi+\delta\phi)$ after relaxation, *i.e.* due to the non-affine response of overlaps. We introduce the Delaunay triangulation (DT) of static packings as sketched in Fig. 1, where the particles in contact are connected by red solid lines and the nearest neighbors without contact, *i.e.* a *virtual contact*, are connected by blue dashed lines. Since the DT is unique for each packing, virtual contacts are uniquely determined and the total number of contacts and virtual contacts are finite. Figures 1(a) and (b) show the DTs before compression and after compression and relaxation, respectively, where the overlaps between virtual contacts are defined as negative values and all kinds of transitions of overlaps are displayed. The overlaps $x_{12}(\phi) > 0$ and $x_{13}(\phi) < 0$ change to $x_{12}(\phi + \delta\phi) > 0$ and $x_{13}(\phi + \delta\phi) < 0$, respectively; they do not change their signs and thus contacts are neither generated nor broken. We name these transitions *contact*-to-*contact* (CC) and *virtual*-to-*virtual* (VV), respectively. On the other hand, $x_{14}(\phi) < 0$ and $x_{15}(\phi) > 0$ change to $x_{14}(\phi + \delta\phi) > 0$ and $x_{15}(\phi + \delta\phi) < 0$, respectively; a new contact is generated and an existing contact is broken, respectively. We name these cases *virtual*-to-*contact* (VC) and *contact*-to-*virtual* (CV), respectively [29].

To characterize all transitions of overlaps, we plot them on scatter plots as shown in Figs. 2(i) and (ii), where $\xi \equiv x(\phi)/\bar{x}(\phi)$ and $\psi \equiv x(\phi + \delta\phi)/\bar{x}(\phi)$ are scaled overlaps before compression and after relaxation, respectively. We also plot the affine response,

$$\psi_{\rm affine} \equiv x_{\rm affine}(\phi + \delta\phi)/\bar{x}(\phi) = \xi + B_{\rm affine}\gamma \ , \quad (1)$$

with the effective increment $\gamma = \delta\phi/(\phi - \phi_J)$ [30] and a coefficient $B_{\rm affine} = d/2\phi A$, where $\psi_{\rm affine}$ is proportional to ξ with an offset linearly dependent on γ. In these figures, the blue and red dots represent $(\xi, \psi_{\rm affine})$ and (ξ, ψ), respectively. Though the overlaps after relaxation

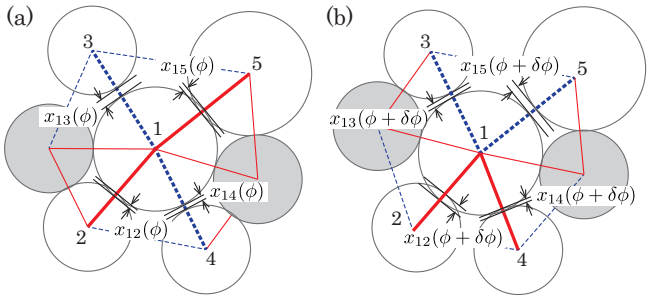

FIG. 1. (Color online) The DTs of static packings (a) before compression (area fraction ϕ) and (b) after compression (area fraction $\phi+\delta\phi$), where the red solid and blue dashed lines represent contacts and virtual contacts, respectively. The open and filled circles are granular particles of which centers are placed on the Delaunay vertices.

are not affine, the deviation of ψ from $\psi_{\rm affine}$ is quite small if the increment $\delta\phi$ is small and the system is far from the jamming point, *i.e.* for $\gamma \ll 1$ (Fig. 2(i)). However, if we increase $\delta\phi$ or decrease $\phi - \phi_J$, ψ deviates visibly from the deterministic prediction $\psi_{\rm affine}$ and data points are more dispersed (Fig. 2(ii)). Figure 2(iii) is a sketch of the differences between affine and non-affine responses, where the mean values in (CC) ξ,$\psi > 0$ and (VV) ξ,$\psi < 0$ are described by linear fitting functions for ψ

$$\text{(CC)} \quad \bar{\psi}_1(\xi) = (a_1 + 1)\xi + b_1 \ , \quad (2)$$

$$\text{(VV)} \quad \bar{\psi}_2(\xi) = (a_2 + 1)\xi + b_2 \ , \quad (3)$$

respectively. The systematic deviation from $\psi_{\rm affine}$ is represented by the differences in slopes (a_1 and a_2) and the offsets (b_1 and b_2). We also introduce standard deviations of ψ from $\bar{\psi}_1(\xi)$ and $\bar{\psi}_2(\xi)$ as v_1 and v_2, respectively, which are almost independent of the initial values ξ. Figure 2(iv) displays a double logarithmic plot of a_1 against γ, where all data collapse onto $a_1 \simeq A_1\gamma$ with $A_1 = 0.76 \pm 0.002$. We also find $a_2 \simeq 0$, $b_1 \simeq B_1\gamma$, $b_2 \simeq B_2\gamma$, $v_1 \simeq V_1\gamma$, and $v_2 \simeq V_2\gamma$ with $B_1 = 0.24 \pm 0.002$, $B_2 = 1.40 \pm 0.001$, $V_1 = 0.32 \pm 0.01$, and $V_2 = 4.41 \pm 0.06$, respectively, within the fitting range $10^{-6} \leq \gamma \leq 1$. Surprisingly, all parameters characterizing not only the mean values, but also the fluctuations are linearly scaled by γ [31]. Because B_2 is comparable to the mean of $B_{\rm affine}$ ($\simeq 1.3$), virtual contacts behave affine in average except for their huge fluctuations around the mean value. In contrast, B_1 is always smaller than $B_{\rm affine}$ and $\bar{\psi}_1(\xi)$ intersects $\psi_{\rm affine}$ at $\xi^* = (B_{\rm affine} - B_1)/A_1 \simeq 1.4$ independent of γ. This leads to small responses ($\psi < \psi_{\rm affine}$) of small overlaps ($0 < \xi \lesssim \xi^*$), which implies preferred tangential and hindered normal displacements as a sign of non-affine deformations [25, 32]. The scattered data in (VC) and (CV) are concentrated in the narrow regions (the inside of the dashed lines in Fig. 2(iii)), while $\psi_{\rm affine}$ linearly increases with ξ in (VC) and there is no data in (CV).

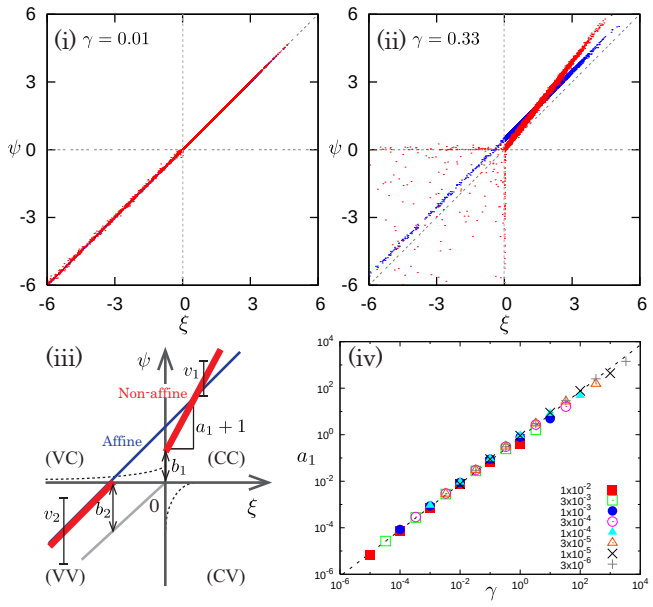

FIG. 2. (Color online) (i) and (ii): Scatter plots of overlaps, where the blue and red dots are $(\xi, \psi^{\rm affine})$ and (ξ, ψ), respectively. Here, $\delta\phi = 4 \times 10^{-5}$ and $\phi - \phi_J =$ (i) 4×10^{-3} and (ii) 1.2×10^{-4}, with $\gamma =$ (i) 0.01 and (ii) 0.33, respectively. (iii): A sketch of deviations from an affine response, where the blue and red solid lines represent $\psi_{\rm affine}$ (for small and large particles) and $\bar{\psi}_1(\xi)$ or $\bar{\psi}_2(\xi)$, respectively. (iv): Double logarithmic plot of a_1 against γ, where the different symbols represent $\phi - \phi_J$ and we change $\delta\phi$ from 10^{-6} to 10^{-2}.

Regarding the overlaps ξ and ψ as two stochastic variables, we introduce a conditional probability distribution (CPD) of the overlaps, $W(\psi|\xi)$, as

$$P_{\phi+\delta\phi}(\psi) = \int_{-\infty}^{\infty} W(\psi|\xi) P_\phi(\xi) d\xi \ , \qquad (4)$$

satisfying a normalization condition $\int_{-\infty}^{\infty} W(\psi|\xi) d\psi = 1$ [33], where $P_\phi(\xi)$ and $P_{\phi+\delta\phi}(\psi)$ are the PDFs of overlaps before and after compression, respectively; $W(\psi|\xi)$ gives a probability distribution of ψ, which was ξ before compression, and can be defined in (CC), (VV), (VC) and (CV). Figure 3(a) shows the CPDs in (CC), where all results with a wide range of γ collapse if we scale $W_{CC}(\psi|\xi)$ and $\psi - \bar{\psi}_1(\xi)$ by γ and $1/\gamma$, respectively. The solid line is a Gaussian distribution function

$$\gamma W_{CC}(\psi|\xi) = \frac{1}{\sqrt{2\pi V_1^2}} \, e^{-\Theta^2/2V_1^2} \qquad (5)$$

with $\Theta \equiv (\psi - \bar{\psi}_1(\xi))/\gamma$. Figure 3(b) displays the CPDs in (VV), where all results collapse as well, after the same scaling as for (CC). The solid line is here the stable distribution function [34]

$$\gamma W_{VV}(\psi|\xi) = \frac{1}{2\pi} \int_{-\infty}^{\infty} e^{-\left(\kappa|V_2 z|^\lambda + i\Omega z\right)} dz \ , \qquad (6)$$

with $\Omega \equiv (\psi - \bar{\psi}_2(\xi))/\gamma$ and a dimensionless wave number z, where the fitting parameters are given by $\lambda = 1.65$ and $\kappa = 0.62$, *i.e.* the CPDs in (VV) are nearly Holtsmark distributions ($\lambda = 3/2$). Figures 3(c) and (d) show the CPDs in (VC) and (CV) approximated by

$$\gamma W_{VC}(\psi|\xi) = \frac{e^{-\Lambda/q_1}}{q_1} \left(1 - \int_{-\infty}^{0} W_{VV}(\psi|\xi) d\psi\right) \ , \qquad (7)$$

$$\gamma W_{CV}(\psi|\xi) = \frac{e^{\Lambda/q_2}}{q_2} \left(1 - \frac{1}{2}{\rm erfc}\left[-\frac{\bar{\psi}_1(\xi)}{\sqrt{2}v_1}\right]\right) \ , \qquad (8)$$

with $\Lambda \equiv \psi/\gamma$ and dimensionless length scales, $q_1 = 0.65$ and $q_2 = 6.10$, respectively. The terms in parentheses on the right hand sides are required to satisfy the normalization conditions [35] and well describe the dependence on ξ (data are not shown). Note that the CPDs in (CC) and (VV) (Eqs. (5) and (6)) converge to a delta-function $\delta(\xi - \psi)$ and those in (VC) and (CV) (Eqs. (7) and (8)) vanish in the limit of $\gamma \to 0$ [36].

Now, we restrict $\delta\phi$ to quite small values compared to $\phi - \phi_J$ and define an infinitesimal effective increment $\delta\gamma \equiv \delta\phi/(\phi - \phi_J) \ll 1$. Introducing a transition rate as $T(\psi|\xi) = W(\psi|\xi)/\delta\gamma$, we rewrite Eq. (4) as the Master equation [33],

$$\frac{\partial}{\partial\gamma} P_\phi(\psi) = \int_{-\infty}^{\infty} \left[T(\psi|\xi) P_\phi(\xi) - T(\xi|\psi) P_\phi(\psi)\right] d\xi \ . \qquad (9)$$

Figures 4(a) and (b) display the numerical solutions of the Master equation under compression, where the CPDs are given by Eqs. (5)-(8). The increment of the area fraction is fixed to $\delta\phi = 10^{-5}$ so that $\delta\gamma \leq 2.5 \times 10^{-3}$ throughout the numerical integrations. Here, the initial condition is given by the PDF obtained through the MD simulations at $\phi_0 - \phi_J = 4 \times 10^{-3}$ with the area fraction before compression ϕ_0. The overlaps are scaled by the mean overlap at the initial state $\bar{x}(\phi_0)$. Good agreement between the solutions (the red solid lines) and the PDFs from simulations (the open symbols) is established for small $\delta\gamma$ and thus we can confirm the Markov property of overlaps. Exchanging ψ for ξ, we can obtain the CPDs for decompression from $\phi + \delta\phi$ to ϕ. The CPDs in (CC) and (VV) are given by replacing the linear fitting functions, $\bar{\psi}_1(\xi)$ and $\bar{\psi}_2(\xi)$, with $\bar{\xi}_1(\psi) = (\psi - b_1)/(a_1 + 1)$ and $\bar{\xi}_2(\psi) = (\psi - b_2)/(a_2 + 1)$, respectively, and the standard deviations, v_1 and v_2, with $v_1/(a_1 + 1)$ and $v_2/(a_2 + 1)$, respectively. The CPDs for decompression in (VC) and (CV) are given by those for compression in (CV) and (VC), respectively. Figures 4(c) and (d) show the numerical solutions of the Master equation under decompression with $\delta\phi = 10^{-5}$ so that $\delta\gamma \leq 2.5 \times 10^{-3}$, where the initial condition is given by the PDF at $\phi_1 - \phi_J = 4 \times 10^{-2}$ with the area fraction before decompression ϕ_1. From these results, we can confirm the reversibility in the sense that the Master equation well describes the PDFs in both directions for small $\delta\gamma$ (even though the initial state before compression and the final state after decompression

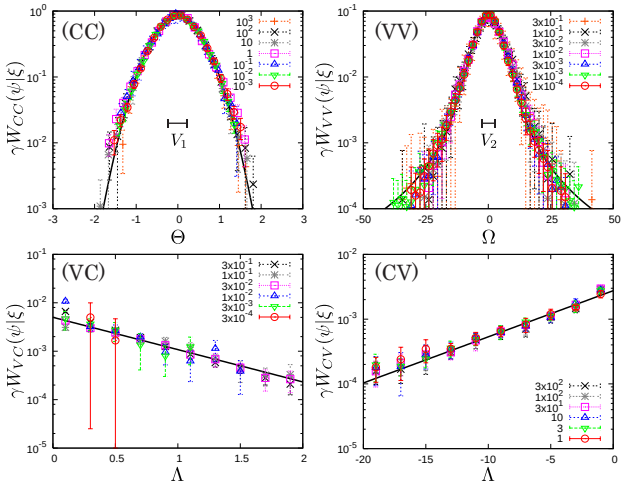

FIG. 3. (Color online) Semi-logarithmic plots of the CPDs in (CC), (VV), (VC), and (CV), against $\Theta = \{\psi - \bar{\psi}_1(\xi)\}/\gamma$, $\Omega = \{\psi - \bar{\psi}_2(\xi)\}/\gamma$ and $\Lambda = \psi/\gamma$, respectively, where we fix $\xi = 1.6$ (CC), -0.2 (VC), and 0.2 (CV), respectively, and average $\gamma W_{VV}(\psi|\xi)$ over $-20 \leq \xi \leq -1$. The different symbols represent the effective increment γ and the solid lines are given by Eqs. (5)-(8).

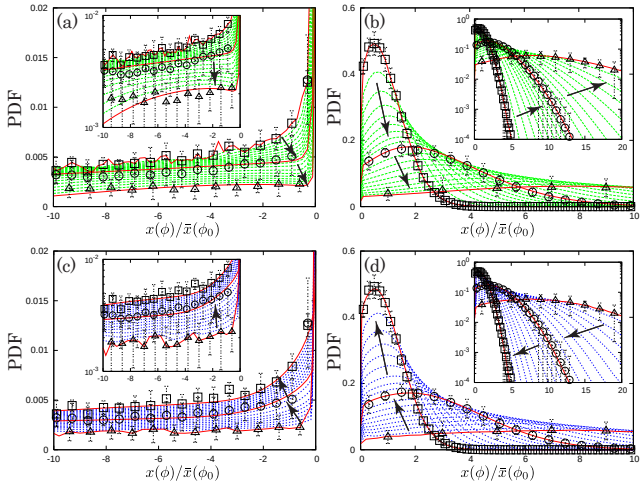

FIG. 4. (Color online) Numerical solutions of the Master equation (the solid and dotted lines) under compression ((a) and (b)) and decompression ((c) and (d)). The solutions develop in the directions indicated by the arrows. The open squares, circles, and triangles are the PDFs obtained through MD simulations at $\phi - \phi_J = 4 \times 10^{-3}$, 1.2×10^{-2}, and 4×10^{-2}, respectively. The insets show the semilogarithmic plots. Overlaps are scaled by the mean overlap at $\phi_0 - \phi_J = 4 \times 10^{-3}$.

are not exactly the same). Note that a similar criterion for the reversibility is found in an experiment of sound propagation in sands [31].

In this study, we provide for the first time the Master equation for the PDFs of overlaps between particles. By considering the extended contact network, the Master equation is able to fully predict the evolution of the PDFs. The novel formulation has a huge impact from the application point of view as it provides a complete statistical description of the stress field in a granular assembly, basis for a macroscopic, continuum, approach to large scale problems. Both the Markov property and reversibility are well retained only if the applied strain increment is infinitesimally small [37]. That is, by including contacts, virtual contacts and their mutual exchange into the description, the behavior is independent on history and the actual stress state is sufficient to predict the subsequent incremental response.

The CPDs show by themselves important properties. While the mean change of overlap reflects non-affine deformations, the Gaussian CPDs in (CC) imply independent stochastic evolution of overlaps/forces around mean values so that they behave independent variables as reported, *e.g.* in Refs. [38, 39]. In contrast, the CPDs in (VV), where no force acts on particles by virtual contacts, is nearly the Holtsmark distribution with much broader tails than the Gaussian, *i.e.* much larger jumps of negative overlaps can occur. This indicates a strongly correlated stochastic evolution of negative overlaps over a wide range of length-scales. Because both the Gaussian and Holtsmark distributions are members of the stable distribution family, fluctuations of contacts and virtual contacts in granular materials do obey the generalized central limit theorem [34]. In addition, the strong deviation from an affine approximation [25] and the large fluctuation of overlaps near the jamming transition [7] in both, contact and virtual contact regimes, are captured by the linear scalings with the effective increment.

Clearly, there is the need of further studies on the physical origin of the non-affine behavior of overlaps and the surprising scaling described above. The origin of the functional forms of the CPDs can give very interesting insights to the mechanics of granular materials, *e.g.* stochastic processes of overlaps. Now, analytic solutions or asymptotic solutions of the Master equation are important possible steps towards the understanding of the functional forms of the PDFs. The Master equation, however, requires the increment $\delta\phi$ to be much smaller than $\phi - \phi_J$. Thus, it can never reach ϕ_J, and the initial condition cannot be the PDF at ϕ_J. This means that the jamming transition is a singular limit of the Master equation. Though the force ensemble theories are restricted to two dimensions [12–14, 40], our analysis can be easily extended to three dimensions and examined by experiments, *e.g.* an oedometer test of sands [41].

We thank M. van Hecke, B. Tighe, H. Hayakawa, S. Yukawa, T. Hatano, H. Yoshino, and K. Kanazawa for fruitful discussions. This work was financially supported by the NWO-STW VICI grant 10828 and a part of numerical computation has been carried out at the Yukawa Institute Computer Facility, Kyoto, Japan.

[1] H. Jaeger, S. R. Nagel, and R. P. Behringer, Rev. Mod. Phys. **68**, 1259 (1996).

[2] C. S. O'Hern, L. E. Silbert, A. J. Liu, and S. R. Nagel, Phys. Rev. E **68**, 011306 (2003).

[3] T. S. Majmudar, M. Sperl, S. Luding, and R. P. Behringer, Phys. Rev. Lett. **98**, 058001 (2007).

[4] M. van Hecke, J. Phys.: Condens. Matter **22**, 033101 (2010).

[5] C. P. Goodrich, A. J. Liu, and S. R. Nagel, Phys. Rev. Lett. **109**, 095704 (2012).

[6] S. F. Edwards and R. B. S. Oakeshott, Physica A **157**, 1080 (1989).

[7] S. Henkes and B. Chakraborty, Phys. Rev. Lett. **95**, 198002 (2005).

[8] B. P. Tighe, J. H. Snoeijer, T. J. H. Vlugt, and M. van Hecke, Soft Matter **6**, 2908 (2010).

[9] R. Blumenfeld and S. F. Edwards, Phys. Rev. Lett. **90**, 114303 (2003).

[10] K. Wang, C. Song, P. Wang, and H. A. Makse, Phys. Rev. E **86**, 011305 (2012).

[11] J. G. Puckett and K. E. Daniels, Phys. Rev. Lett. **110**, 058001 (2013).

[12] P. T. Metzger, Phys. Rev. E **70**, 051303 (2004).

[13] S. Henkes, C. S. O'Hern, and B. Chakraborty, Phys. Rev. Lett. **99**, 038002 (2007).

[14] B. P. Tighe, A. R. T. van Eerd, and T. J. H. Vlugt, Phys. Rev. Lett. **100**, 238001 (2008).

[15] J. M. Erikson, N. W. Mueggenburg, H. M. Jaeger, and S. R. Nagel, Phys. Rev. E **66**, 040301(R) (2002).

[16] E. I. Corwin, H. M. Jaeger, and S. R. Nagel, Nature **435**, 1075 (2005).

[17] K. W. Desmond, P. J. Young, D. Chen, and E. R. Weeks, Soft Matter **9**, 3424 (2013).

[18] L. E. Silbert, G. S. Grest, and J. W. Landry, Phys. Rev. E **66**, 061303 (2002).

[19] J. W. Landry, G. S. Grest, L. E. Silbert, and S. J. Plimpton, Phys. Rev. E **67**, 041303 (2003).

[20] M.-K. Müller, S. Luding, and T. Pöschel, Chem. Phys. **375**, 600 (2010).

[21] A. R. T. van Eerd, W. G. Ellenbroek, M. van Hecke, J. H. Snoeijer, and T. J. H. Vlugt, Phys. Rev. E **75**, 060302(R) (2007).

[22] M. Wyart, Phys. Rev. Lett. **109**, 125502 (2012).

[23] E. Lerner, G. Düring, and M. Wyart, Soft Matter **9**, 8252 (2013).

[24] P. Charbonneau, E. I. Corwin, G. Parisi, and F. Zamponi, Phys. Rev. Lett. **109**, 205501 (2012).

[25] W. G. Ellenbroek, M. van Hecke, and W. van Saarloos, Phys. Rev. E **80**, 061307 (2009).

[26] The static packings prepared with longer length scales $l = 10^3 R$ and $10^4 R$ give the same results concerning critical scaling of frictionless particles near the jamming point [2–4], while we cannot obtain the same results with a smaller value $l = 10R$.

[27] P. J. Digby, J. Appl. Mech. **48**, 803 (1981).

[28] We neglect the higher order term $x(\phi)\delta\phi$.

[29] In our simulations, the total number of contacts and virtual contacts are independent of the area fraction and always conserved under both compression and decompression. Although we do not take into account *flips* of Delaunay edges by large displacements of particles, we have not observed any flips if $\gamma < 0.01$ and the number of flipped edges are less than 2% at most for $\gamma = 3 \times 10^3$.

[30] γ can be large, whereas $\delta\gamma$ is always small.

[31] T. Brunet, X. Jia, and P. A. Johnson, Geophys. Res. Lett. **35**, L19308 (2008).

[32] O. D. N. P. Kruyt and S. Luding, Int. J. Sol. Struct. **47**, 2234 (2010).

[33] N. G. van Kampen, *Stochastic Processes in Physics and Chemistry, 3rd edition* (Elsevier B. V. Amsterdam, The Netherlands, 2007).

[34] J. Voit, *The Statistical Mechanics of Financial Markets, 3rd Edition* (Springer-Verlag, Berlin, 2005).

[35] The normalization condition is given by $\int_{-\infty}^{0} W_{VV} d\psi + \int_{0}^{\infty} W_{VC} d\psi = \int_{-\infty}^{0} W_{CV} d\psi + \int_{0}^{\infty} W_{CC} d\psi = 1$.

[36] We rewrite $W_{VV} = (2\pi)^{-1} \int e^{-\left[\kappa|\gamma V_2 z|^\lambda + i(\psi - \bar{\psi}_2)z\right]} dz$ and take $\lim_{\gamma\to 0} W_{VV} = (2\pi)^{-1} \int e^{i(\xi-\psi)z} dz = \delta(\xi - \psi)$, where we used $\lim_{\gamma\to 0} \bar{\psi}_2 = \xi$. Because of $\lim_{X\to 0} e^{-1/X}/X = 0$, the CPDs in (VC) and (CV) vanish in the limit of $\gamma \to 0$.

[37] K. Saitoh, V. Magnanimo, and S. Luding, in preparation.

[38] N. P. Kruyt and L. Rothenburg, Int. J. Solids Struct. **39**, 571 (2002).

[39] T. S. Majmudar and R. P. Behringer, Nature **435**, 1079 (2005).

[40] S. Sarkar, D. Bi, J. Zhang, R. P. Behringer, and B. Chakraborty, Phys. Rev. Lett. **111**, 068301 (2013).

[41] Y.-H. Wang and Y. Gao, Granular Matter. DOI 10.1007/s10035-013-0457-1.